Surface erosion in nc-ZrN/a-ZrCu multilayer films after He irradiation

V.V. Uglov [a, b], G. Abadias [c], S.V. Zlotski [a], I.A. Saladukhin [a], I.S. Veremei [a]

[a] Belarusian State University, Minsk 220030, Nezavisimosti ave., 4, Belarus [b] Tomsk Polytechnic University, Tomsk 634028, Lenina ave., 2a, Russia

[c] Institut Pprime, UPR 3346 CNRS-Université de Poitiers- ENSMA, 11 Boulevard Marie et Pierre Curie, TSA 41123, 86073 Poitiers Cedex 9, France

ARTICLE INFO

Keywords:
Magnetron sputtering
Multilayered films
Ion irradiation
Blistering and flaking

ABSTRACT

The work is dedicated to the study of the phase stability and surface erosion of a novel Zr-based multilayer system consisting of a combination of ceramic (ZrN) and metallic glass (Zr—Cu) nanoscale layers after He irradiation (40 keV and doses up to 1.1 × 10^{18} cm^{-2}). Periodic ZrN/$Zr_{1-x}Cu_x$ multilay-ers with elementary layer thicknesses of 5 nm/5 nm and 5 nm/10 nm and Cu content x = 0.45, 0.53, 0.61 and 0.74 were grown by magnetron sputter-deposition from Zr and Cu targets at the substrate temperature of 300 °C. X-ray diffraction and X-ray reflectivity analysis reveal that multilayered films consist of alternating nanocrys-talline (nc) ZrN and amorphous (a) ZrCu layers with relatively sharp interfaces. The stability of the phase compo-sition of nc-ZrN/a-$Zr_{1-x}Cu_x$ multilayer films to irradiation with helium ions up to fluence of 1.1 × 10^{18} cm^{-2} has been established. For x = 0.74, crystallization of the metallic glass layer was observed.

The surface integrity of the multilayer films remained unaltered up to an ion fluence of 5 × 10^{17} cm^{-2}. At higher ion fluence, surface erosion of the nc-ZrN/a-$Zr_{1-x}Cu_x$ films occurs by the flacking mechanism. In this case, an increase in the thickness of the amorphous $Zr_{1-x}Cu_x$ layer and in Cu content leads to improved radiation resis-tance as the critical fluence for delamination increases from 5 × 10^{17} cm^{-2} upto 8 × 10^{17} cm^{-2}.

1. Introduction

Nowadays the development of new radiation-resistant materials is a crucial problem that is especially urgent for fission/fusion industry, aerospace application, etc., wherein objects are exposed to strong irra-diation with ions, neutrons, or electrons. For instance, irradiation with light ions due to nuclear collisions can induce a higher ratio of point de-fects (e.g. vacancies and interstitials) relatively to defect clusters (e.g. He bubbles) in metallic crystals [1,2]. This in turn remarkably degrades the performance of structural materials in advanced fission/fusion reac-tors, which must be significantly improved to extend their reliability and efficiency [3,4]. Because of the detrimental effects of radiation-induced defects and He accumulation from transmutation reactions on materials mechanical properties, radiation environments pose a great challenge for materials scientists in terms of choosing and designing materials that resist radiation damage while maintaining high strength and toughness.

Therefore, it becomes necessary to design materials with a large number of sinks for point defects, such as dislocations, grain bound-aries, and interphase boundaries to achieve this goal [5,6]. Nanostruc-tured materials, such as nanocrystalline [7,8] and multilayer materials [9,10], contain abundant interfaces, which can serve as effective defect sinks to absorb irradiation-generated defects and relieve radiation dam-age [11]. Multilayer systems are promising for research because inter-layer boundaries can affect the removal of radiation-induced defects. They have significant interphase regions, which can act as stable sinks of defects. Misra et al. [12] showed that Cu/Nb layer interfaces curtail the nucleation and growth of He bubbles. The ability of layer interfaces to trap defect clusters and reduce radiation damage has also been re-ported in other systems, such as Cu/V [13], Al/Nb [14], Cu/Mo [15], and Fe/W [16]. Generally, the reduction in layer thickness leads to en-hanced radiation performance due to the increasing density of layer in-terfaces.

One of the most promising materials with a large number of grain boundaries are nanocrystalline (nc) coatings, for example nc-ZrN, formed by vacuum arc deposition [17]. The deposited layers can ex-hibit a susceptibility to blistering that is dependent on the layer struc-ture and composition, as well as on the presence of interfaces. Along with crystalline/crystalline systems outlined above, nanostructured coatings with crystalline/amorphous (nc/a) interfaces (such as ZrSiN nanocomposite and nc-MeN/a-Si_3N_4 multilayers, with Me = Zr, Al or Cr) exhibit a high radiation tolerance, and resistance to surface erosion

Table 1
Characteristics of nc-ZrN/a-ZrCu multilayers: thickness ratio of ZrN and ZrCu elementary layers, total film thickness, range of He ions.

Zr power (W)	Cu power (W)	Cu content in $Zr_{1-x}Cu_x$ layer	Total film thickness (nm)		Projected range R_p of He ions calculated by SRIM (nm)	
			ZrN (5 nm)/ ZrCu (5 nm)	ZrN (5 nm)/ ZrCu (10 nm)	ZrN (5 nm)/ ZrCu (5 nm)	ZrN(5 nm)/ ZrCu (10 nm)
294	40	0.45	298	302	153	159
243	51	0.53	296	300	153	158
164	51	0.61	299	301	152	156
88	51	0.74	292	296	152	154

due to amorphous nanolayers associated with excellent defects absorp-tion capability [18–21]. Zhang et al. [22] showed size-dependent radia-tion tolerance of Cu/a-ZrCu nanolaminates against He implantation. Yu et al. [23] showed that irradiation-induced Fe/a-FeZr interfaces could absorb defects and confine the movement of dislocation loops in crys-talline layers to annihilate opposite defects under in situ Kr ion irradia-tion. However, the questions such as irradiation-induced grain growth, phase stability of amorphous layers, and effect of crystalline/amor-phous interfaces on radiation tolerance remain to be elucidated further.

This article is devoted to the study of the radiation resistance of a novel class of

nc/a multilayer system alternating nanoscale ceramic (ZrN) and metallic glass ($Zr_{1-x}Cu_x$) layers. To this end, the phase composition and surface erosion of nc-ZrN/a-$Zr_{1-x}Cu_x$ multilayers with bilayer periods of 10 and 15 nm and various Cu content x (in the 0.45–0.74 range) irradi-ated with helium ions with a fluence up to $1.1 \times 10_{18}$ cm_{-2} were inves-tigated by combining X-ray diffraction (XRD) and scanning electron mi-croscopy (SEM).

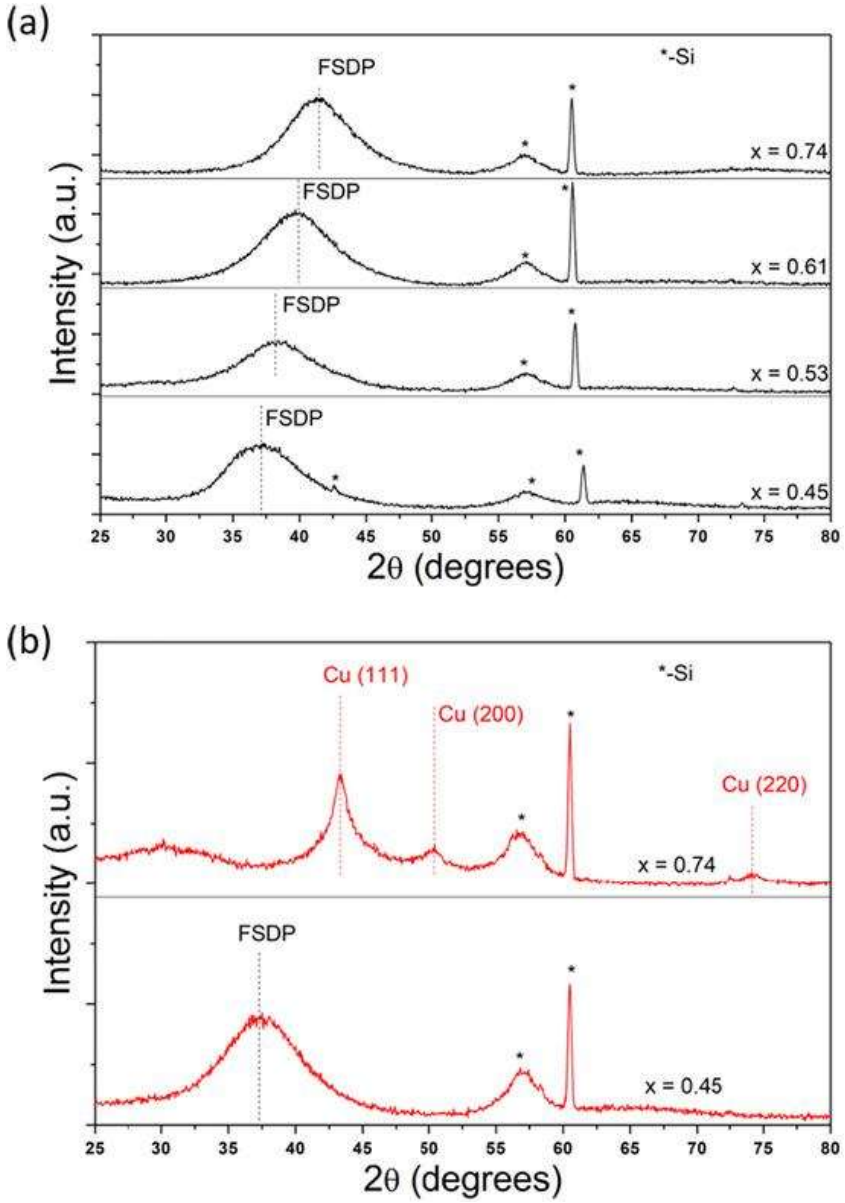

Fig. 1. XRD patterns of (a) as-deposited and (b) irradiated with 40 keV He_{2+} ions at fluence of $1.1 \times 10_{18}$ cm_{-2} $Zr_{1-x}Cu_x$ films with different Cu concentration x. XRD patterns were obtained at an X-ray beam incidence angle of 5°.

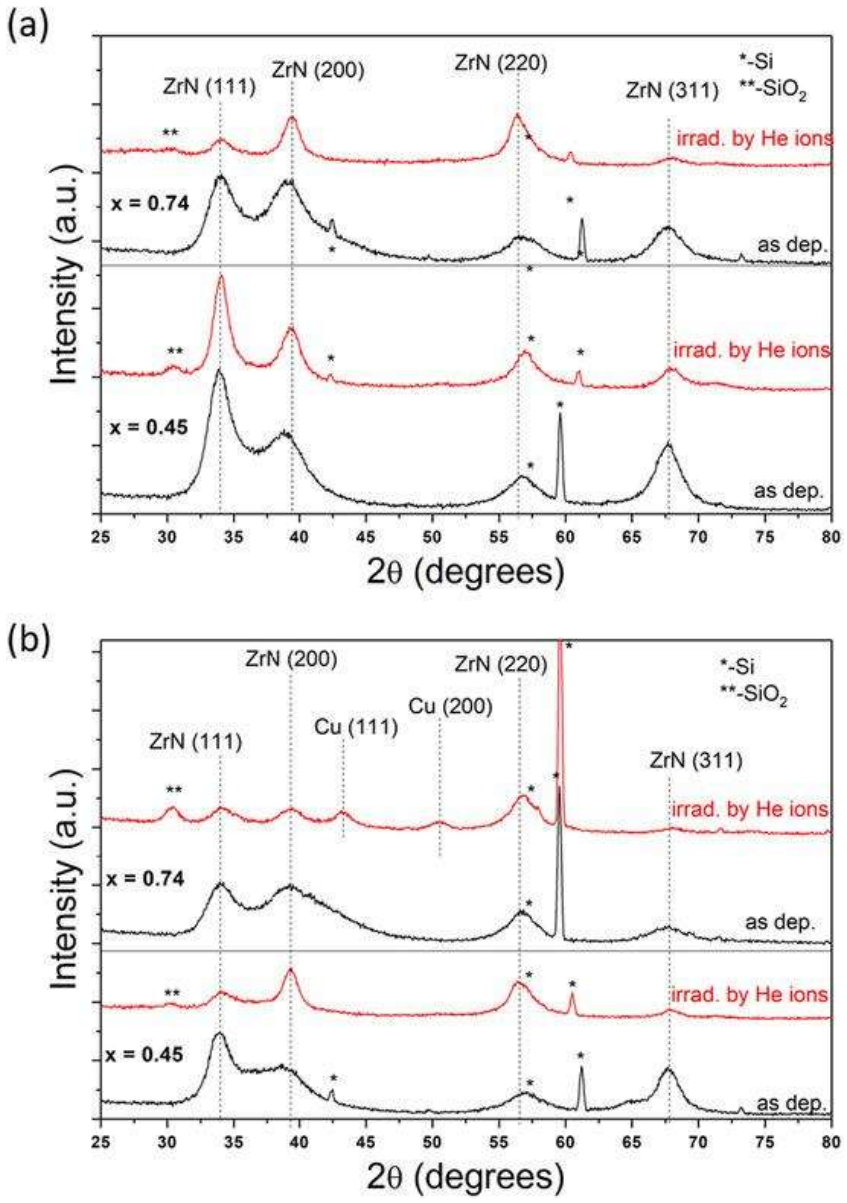

Fig. 2. XRD patterns of as-deposited (black line) and irradiated (red line) with 40 keV He^{2+} ions at fluence of 1.1×10^{18} cm^{-2} nc-ZrN/a-$Zr_{1-x}Cu_x$ multilayer films with (a) 5 nm/5 nm and (b) 5 nm/10 nm bilayer period and Cu concentration x = 0.45 and x = 0.74. XRD patterns were obtained at an X-ray beam incidence angle of 5°.

2. Experimental details

nc-ZrN/a-ZrCu multilayer films were grown at a nominal temperature of 300 °C by magnetron sputter-deposition in a high-vacuum chamber (base pressure < 10^{-5} Pa) equipped with three confocal targets and a cryogenic pump (max. 500 l/s). Films were deposited on Si (100) substrates covered with 10 nm thick thermally grown SiO_2 amorphous layer. A constant bias voltage of −60 V was applied to the substrate during deposition, while the substrate was rotated at 15 rpm throughout the whole deposition to ensure an equal deposition rate across the substrate area. The temperature measured by the mean of a thermocouple in the vicinity of the substrate position was 300 °C.

Water-cooled, 7.62-cm-diameter Zr (99.92% purity) and Cu (99.9% purity) targets, located at 18 cm from the substrate holder, were oper-ated at constant power mode using a DC power supply and unbalanced magnetic configuration. A pure Ar discharge was used for the growth of $Zr_{1-x}Cu_x$ layers obtained by co-deposition, while a mixed Ar/N_2 plasma was employed to deposit ZrN layers by reactive sputtering (in metallic target mode). The total working pressure was 0.21 Pa, as measured us-ing a Baratron® capacitance gauge. The Ar/N_2 flow ratio was optimized to obtain a Zr/N ratio close to 1.0 (stoichiometry) based on earlier results [24]. The N_2 partial pressure was measured and controlled during deposition using a MKS Microvision mass spectrometer.

nc-ZrN/a-$Zr_{1-x}Cu_x$ multilayer films with different Cu content x and thickness of ZrN and $Zr_{1-x}Cu_x$ elementary layers have been investigated. The Cu content in the $Zr_{1-x}Cu_x$ layers was varied by changing the DC power supply of the Cu target, from 40 to 52 W, and the DC power sup-ply of Zr target, from 88 up to 294 W. As a result, $Zr_{1-x}Cu_x$ layers with x content ranging from 0.45 to 0.74 were synthesized, as determined from elemental probe microanalysis. The main characteristics of the in-vestigated nc-ZrN/a-$Zr_{1-x}Cu_x$ multilayer films are listed in Table 1.

The periodic growth of ZrN/$Zr_{1-x}Cu_x$ layered stack was monitored by computer-controlled pneumatic shutters located at 2 cm in front of each target. The deposition process always started with the $Zr_{1-x}Cu_x$ sub-layer being deposited first. A holding time of 10 s was included in the growth sequence to pump N_2 gas before $Zr_{1-x}Cu_x$ deposition. The to-

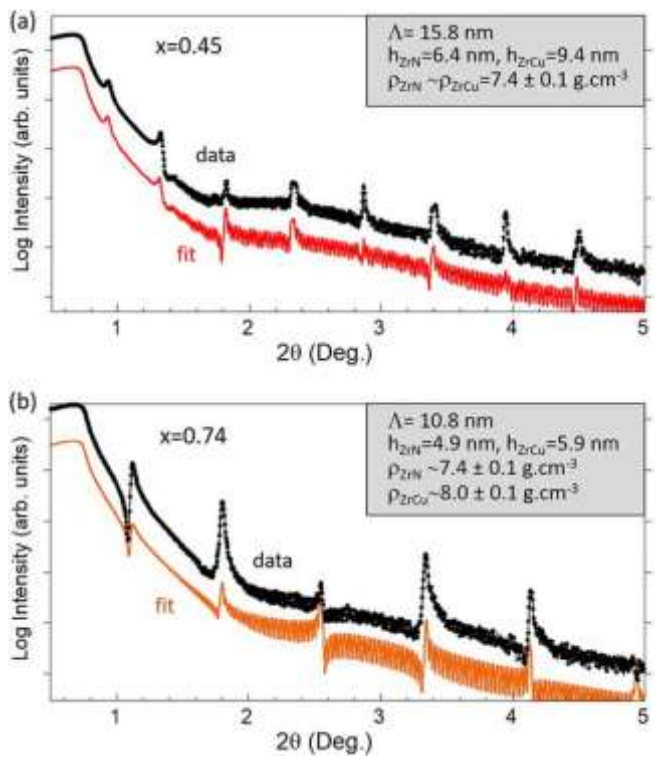

Fig. 3. XRR patterns of as-deposited (a) nc-ZrN/a-$Zr_{1-x}Cu_x$ (5 nm/10 nm, x = 0.45) and (b) nc-ZrN/a-$Zr_{1-x}Cu_x$ (5 nm/5 nm, x = 0.74) multilayer films. Best-fit simulations to experimental data are shifted for better clarity.

Table 2
The critical fluence of blister formation or flaking of nc-ZrN/a-$Zr_{1-x}Cu_x$ multi-layer irradiated by He (40 keV) ions.

Cu content in $Zr_{1-x}Cu_x$ layer	The critical fluence of blister formation or flaking of multilayers, cm^{-2}	
	ZrN (5 nm)/ZrCu (5 nm)	ZrN (5 nm)/ZrCu (10 nm)
0.45	$5 \times 10_{17}$	$6 \times 10_{17}$
0.53	$5 \times 10_{17}$	$7 \times 10_{17}$
0.61	$5 \times 10_{17}$	$7 \times 10_{17}$
0.74	$5 \times 10_{17}$	$8 \times 10_{17}$

tal film thickness was about 300 nm (Table 1). Another film series, namely 300 nm thick $Zr_{1-x}Cu_x$ monolithic films with the same elemental composition as in multilayer series, was also prepared for reference purpose.

Ion implantation of the nc-ZrN/a-$Zr_{1-x}Cu_x$ multilayered films was carried out using 40 keV He^{2+} ions at the DC-60 heavy-ion accelerator at the fluence from $3.0 \times 10_{17}$ upto $1.1 \times 10_{18}$ cm^{-2}. Irradiation with helium ions was perpendicular to the surface of the samples. The implantation temperature was 300 K. The beam current was 20 μA, and water cooling of the target substrate was used. The energetic parameters of implantation were chosen so as the implanted He distribution depth did not exceed the film thickness, as calculated using the SRIM-2012 code [25].

X-ray Diffraction (XRD) analysis was employed for structural identification using an Ultima IV Rigaku X-ray diffractometer operating in parallel configuration and equipped with CuKα wavelength (0.15418 nm). XRD scans were collected at an incidence angle of 5°. X-ray reflectivity scans were measured using a Seifert XRD 3000 diffrac-tometer equipped with a line focus Cu source, a channel cut Ge (220) monochromator, and a scintillation detector defined with a resolution slit of 0.07 mm. An optical model, based on Parratt's formalism, was fit-ted to experimental data to obtain information on the bilayer period Λ, individual layer thickness (h_{ZrN} and h_{ZrCu}) and mass density (ρ_{ZrN} and ρ_{ZrCu}) of constitutive layers using a refinement procedure.

The morphology of the films surface was studied by scanning electron microscopy (SEM) on plan-view specimens using a JEOL JSM-7500F Field Emission Scanning Electron Microscope. The films thickness was determined from cross-section SEM micrographs analysis.

3. Results

3.1. As-deposited films state

Fig. 1a displays the XRD patterns of as-deposited monolithic $Zr_{1-x}Cu_x$ reference films with Cu content x = 0.45, 0.53, 0.61 and 0.74. For all films, the presence of a broad halo, characteristic of the first sharp diffraction peak (FSDP) in metallic glasses [26–28], is observed. This indicates the formation of amorphous films in the investigated compositional range. The position of the FSDP is related to the medium-range order in amorphous alloys, i.e. to the correlations between atomic clusters [28,29]. For bulk metallic glasses, the position $4\pi\sin\theta$ of the FSDP is closely related to the average atomic volume V_a, following a universal scaling law $q \sim V_a^{-0.443}$ [29]. This relation was also observed for Zr—*Cu thin film metallic glasses, suggesting that the driving force for the alloy internal atomic structure is primarily gov-erned by the composition [28]. In our case, the angular position of the FSDP changes from 37.15 to 41.35° with increasing Cu content x from 0.45 to 0.74. Using Bragg's relation, the equivalent interplanar spacing (d) for Zr—Cu films is found to decrease from about 0.2417 nm to 0.2173 nm. Since the radius of the Cu atom (0.128 nm) is smaller than the radius of the Zr one (0.160 nm), the substitution of zirconium for copper leads to a decrease in the bonding length. The change in bond-ing length also depends on the degree of short- and medium-range or-der. The presence of polyhedral-type short- and medium-range ordering structures in amorphous alloys is controlled by the atomic size ratio and the electronic interactions between the constitutive elements. For in-stance, for a $Zr_{0.7}Cu_{0.3}$ alloy, Saksl et al. [30] reported from extended x-ray absorption fine structure the existence of short-range ordering around Zr atoms, identifying the formation of icosahedral-like clusters. At x = 0.45, one can notice an asymmetry in the shape of the FSDP, which can be attributed to the overlap between two broad ZrCu diffrac-tion lines, corresponding to (111) and (200) planes, suggesting the pos-sible formation of a nanocrystalline structure. In the remaining of the article, we will present results obtained for the lowest (x = 0.45) and highest (x = 0.74) Cu content investigated.*

XRD patterns of as-deposited nc-ZrN/a-$Zr_{1-x}Cu_x$ (5 nm/5 nm) and nc-ZrN/a-$Zr_{1-x}Cu_x$ (5 nm/10 nm) multilayer films are shown in Fig. 2 for the two extreme Cu content, x = 0.45 and x = 0.74. Diffraction lines corresponding to cubic (Na—Cl type) lattice of ZrN are clearly identified for both investigated bilayer periods. Bragg reflections from (111), (200), (220) and (311) planes are observed, attesting the formation of polycrystalline ZrN layers. The position of these lines remains practically unchanged when the metallic glass layer thickness changes from 5 to 10 nm. One can only note different intensity profile due to the convolution between the FSDP of the $Zr_{1-x}Cu_x$ layer and the diffraction lines from ZrN layer.

Fig. 3 shows the results of XRR studies of multilayer films. Well de-fined superlattice peaks are observed, together with Kiessig's fringes in-between, attesting of the highly periodic compositional profile and the presence of smooth interfaces. The number of these peaks and their spacing depend on the multilayer period Λ, while their intensity and shape are affected by the fraction of metallic glass and the structural disorder (layer thickness fluctuations and roughness). For example, for x = 0.45, due to similar mass densities between ZrN and $Zr_{0.55}Cu_{0.45}$, these superlattice reflections merely emerge from the reflected inten-sity background. Quantitative information on the density and thickness of individual layers were obtained from a fit of XRR scans to an optical

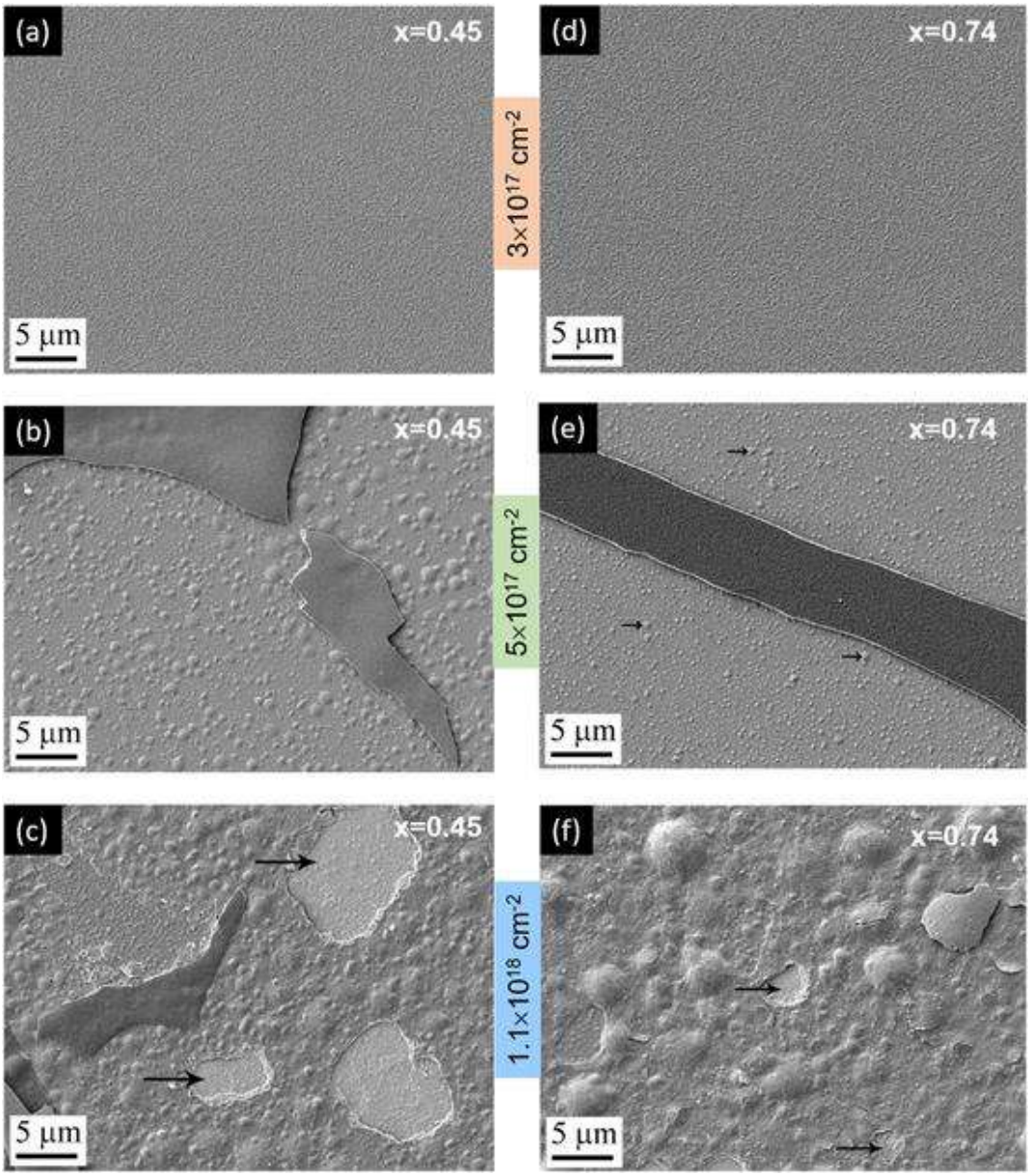

Fig. 4. SEM images of the surface of the nc-ZrN/a-$Zr_{1-x}Cu_x$ (5 nm/5 nm) multilayers with x = 0.45 (a,b,c) and x = 0.74 (d,e,f) irradiated with 40 keV He^{2+} ions at the fluence of 3 × 10^{17} cm^{-2} (a,d), 5 × 10^{17} cm^{-2} (b,e) and 1.1 × 10^{18} cm^{-2} (c,f). Arrows indicate the presence of large blisters.

model, yielding the following values for the selected samples shown in Fig. 3: h_{ZrN} = 6.4 and h_{ZrCu} = 9.4 nm for the nc-ZrN/a-$Zr_{0.55}Cu_{0.45}$ (5 nm/10 nm) multilayer and h_{ZrN} = 4.9 and h_{ZrCu} = 5.9 nm for the nc-ZrN/a-$Zr_{0.26}Cu_{0.74}$ (5 nm/5 nm) multilayer. The extracted ZrN den-sity was 7.4 g/cm_3, and the density of $Zr_{1-x}Cu_x$ increased from 7.4 to 8.0 g/cm_3 with increasing Cu content. These values are consistent with mass density of bulk ZrN (7.4 g/cm_3) and literature values for Zr—Cu thin film metallic glasses [26].

3.2. Irradiated films

Before investigating the surface of irradiated films, calculations using SRIM computer code were performed. For these calculations, the densities of ZrN and ZrCu layers, taken from the XRR investigations were used. The results of SRIM calculations are presented in Table 1, where the projected range of the He distribution, R_p, is reported. The maximum He concentration is found to be located in the ZrN layers. SRIM calculations showed that the mean projected range R_p of He is 152–153 nm for nc-ZrN/a-$Zr_{1-x}Cu_x$ (5 nm/5 nm) and 154–159 nm for nc-ZrN/a-$Zr_{1-x}Cu_x$ (5 nm/10 nm), depending on Cu content, see Table 1. The results of SEM investigations of the nc-ZrN/a-$Zr_{1-x}Cu_x$ multi-layer films irradiated with 40 keV He_{2+} ions in the fluence range from 3.0 × 10_{17} to 1.1 × 10_{18} cm_{-2} allow to experimentally estimate the critical fluence for blister formation or flaking, i.e. the fluence at which the radiation-induced erosion of surface starts. This critical fluence is reported in Table 2 for the investigated samples.

SEM studies of the multilayer films surface showed no blistering or flaking after irradiation with He ions at fluence below 5 × 10_{17} cm_{-2} (Figs. 4a, d, 5a, d and Suppl. File). In the case of nc-ZrN/a-$Zr_{1-x}Cu_x$ (5 nm/5 nm) multilayer films, the critical fluence of surface erosion is equal to 5 × 10_{17} cm_{-2} (Fig. 4b, e). As can be seen from Fig. 4b and e, the surface erosion of the multilayer nc-ZrN/a-$Zr_{1-x}Cu_x$ films (5 nm/ 5 nm) is mainly associated with surface flaking. Rough islands are visible on the surface of the irradiated films. The strongest surface erosion due to flaking is found for a Cu content x = 0.53 (see Suppl. File). Also,

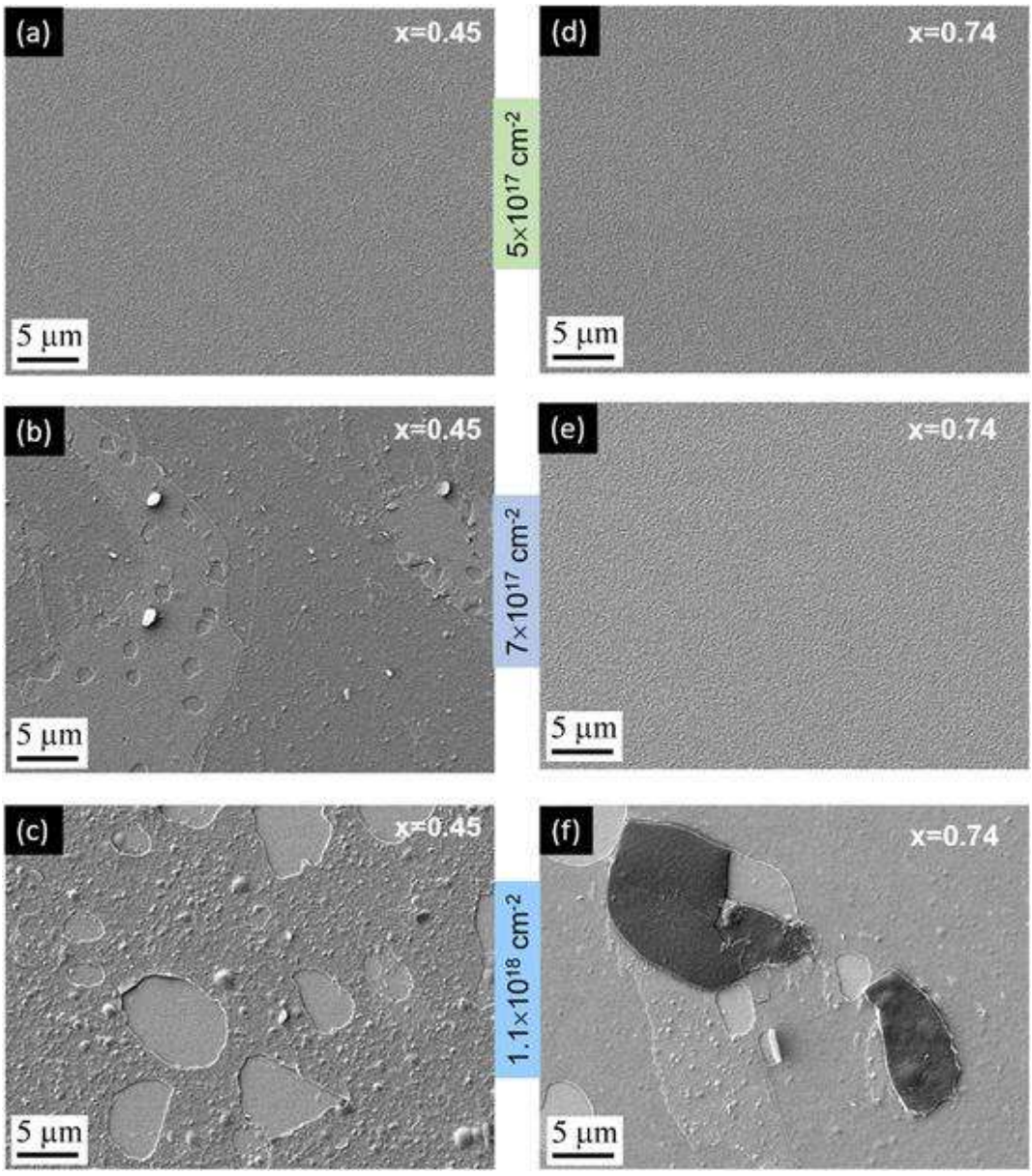

Fig. 5. SEM images of the surface of the nc-ZrN/a-$Zr_{1-x}Cu_x$ (5 nm/10 nm) multilayers with x = 0.45 (a,b,c) and x = 0.74 (d,e,f) irradiated with 40 keV He^{2+} ions at the fluence of 5 × 10^{17} cm^{-2} (a,d), 7 × 10^{17} cm^{-2} (b, e) and 1.1 × 10^{18} cm^{-2} (c,f).

in the areas of the surface after flacking, numerous closed blisters with a diameter ranging from 170 to 180 nm to 0.45–1.14 μm are visible (indicated by arrows). In this case, large blisters are formed as a result of the agglomeration of small ones, which is mainly due to the high density of blister formation. It was found that with an increase in the Cu content in the $Zr_{1-x}Cu_x$ layer, the diameter of large blisters decreases from 1.14 to 0.45 μm (Fig. 4e). This indicates a decrease in the density of blister formation with increasing copper concentration. The formation of small blisters indicates a small depth of their formation, which is associated with the delamination of the film with a thickness corresponding to R_p. A further increase in the fluence of He ions upto 1.1 × 10^{18} cm^{-2} leads to new flacking of the film, as well as the forma-tion of large open blisters with a diameter of 3–4 μm (Fig. 4c, f and Suppl. File). In this case, the erosion of the film surface appears to reach the silicon substrate.

SEM studies of the surface erosion of nc-ZrN/a-$Zr_{1-x}Cu_x$ multilayer films with 5 nm/10 nm period showed an increase in the critical fluence of surface erosion (Fig. 5a, d) compared to nc-ZrN/a-ZrCu films with 5 nm/5 nm period (Fig. 4b, e). It was found that with an increase in the Cu content in the amorphous $Zr_{1-x}Cu_x$ layer from 0.45 to 0.74 the critical fluence of surface erosion increases from 6 × 10^{17} cm^{-2} to 8 × 10^{17} cm^{-2} (see Table 2). At the same time, for all Cu content, the main surface erosion is associated also with the flacking mechanism.

It was found that erosion of the nc-ZrN/a-$Zr_{1-x}Cu_x$ film (5 nm/ 10 nm) with x = 0.45 occurs only by the flaking mechanism (Fig. 5b). For x = 0.53, in addition to flacking, open blisters with a diameter of 1.3 μm are observed (see Suppl. File). The shape of the caps of these blisters indicates a low plasticity of the layer in which the blister is formed. In addition, there are also small-diameter blisters, as for nc-ZrN/a-$Zr_{1-x}Cu_x$ (5 nm/5 nm) films.

Surface erosion in the nc-ZrN/a-ZrCu multilayer film (5 nm/10 nm) with x = 0.61 is mainly characterized by flaking (see Suppl. File). SEM images show areas with multi-level flaking. For the maximum Cu content, x = 0.74, the formation of a large number of small blisters with a diameter of 200–300 nm was also revealed (Fig. 5e).

An increase in the ion fluence to 1.1 × 10_{18} cm_{-2} also leads to the formation of large areas of erosion on the surface of multilayer nc-ZrN/a-$Zr_{1-x}Cu_x$ films (5 nm/10 nm) as a result of flaking of the film surface (Fig. 5c, f and Suppl. File).

To reveal the effect of high fluences of He ions on the structural integrity of

nc-ZrN/a-$Zr_{1-x}Cu_x$ multilayer films, XRD studies of multilayer films irradiated with 40 keV He_{2+} ions at fluence of 1.1 × 10_{18} cm_{-2} were performed. It was found that irradiation at maximum fluence did not shift the position of the ZrN diffraction peaks (Fig. 2). A decrease in the intensity and width of diffraction peaks was revealed, which is associated with surface erosion and stress relaxation. It was found that the ZrN phase is retained at a maximum fluence of 1.1 × 10_{18} cm_{-2} (Fig. 2) and the amorphous $Zr_{1-x}Cu_x$ phase remains stable for x content in the 0.45–0.61 range (see Fig. 1b and Fig. 2). For x = 0.74 and an amorphous layer thickness of 5 nm, the amorphous $Zr_{1-x}Cu_x$ phase remains stable. For x = 0.74 and an amorphous layer thickness greater or equal to 10 nm, crystallization of a Cu-rich phase was revealed (see Fig. 1b and Fig. 2b).

4. Discussion

Surface erosion of nc-ZrN/a-$Zr_{1-x}Cu_x$ multilayer films by flacking is due to the presence of amorphous $Zr_{1-x}Cu_x$ layers. As reported earlier, blister formation in ZrN films can be described on the basis of the mech-anism of inter-bubble fracture [31], which occurs due to the high over-pressure in pores located at depths close to R_p. In our case, the forma-tion of pores likely occurs in amorphous $Zr_{1-x}Cu_x$ layers, in view of their high efficiency in absorbing radiation defects [32]. Helium-vacancy complexes and their clusters diffuse into amorphous layers and dissolve into them to form helium bubbles. This leads to the swelling of the mul-tilayer film without surface erosion. When the critical concentration of helium in the amorphous layers is reached, helium bubbles combine to form other bubbles with a high pressure. This leads to the appearance of longitudinal cracks between the bubbles, which lead to the coalescence of the bubbles, an increase in pressure in them, and further propagation of cracks. This results in flaking of large surface areas (see Figs. 4 and 5). Therefore, an increase in the thickness of the amorphous ZrCu layer leads to an increase in the critical fluence at which the film starts to flake, consistent to our experimental observations. The observed in-crease in the critical fluence in nc-ZrN/a-$Zr_{1-x}Cu_x$ (5 nm/10 nm) multi-layer films with increasing Cu content could be associated with an in-crease in the elastic modulus of $Zr_{1-x}Cu_x$ with x rise [33].

The formation of blisters with a diameter of several hundred nanometers, apparently, occurs in the amorphous layers of ZrCu after flacking off the upper layer. Their small diameter is due to the shallow depth of formation of blister nucleus. Subsequent irradiation with He ions (an increase in the ion fluence) leads to the formation of new bubbles predominantly in the silicon substrate, which causes the formation of large regions of erosion by the flaking mechanism. In some cases, blisters with a diameter of 1.3 μm with an open lid are formed (Fig. 5).

5. Conclusions

nc-ZrN/a-$Zr_{1-x}Cu_x$ multilayer films with different thicknesses of elementary layers and Cu content in $Zr_{1-x}Cu_x$ layers were deposited by magnetron sputtering. The films consist of alternating crystalline ZrN and amorphous $Zr_{1-x}Cu_x$ layers. The formed multilayer films were subsequently irradiated with helium (40 keV) ions at high fluence (up to 1.1 × 10_{18} cm_{-2}).

The stability of the phase composition of nc-ZrN/a-$Zr_{1-x}Cu_x$ multilayer films to irradiation with helium ions up to fluence of 1.1 × 10_{18} cm_{-2} has been established. In this case, at the maximum Cu content x = 0.74 and an amorphous layer thickness greater or equal to 10 nm, crystallization of the metallic Cu-rich phase occurs.

The surface integrity of the multilayered films was maintained for fluence lower than

5 × 10_{17} cm_{-2}. At higher fluence, surface erosion of nc-ZrN/a-$Zr_{1-x}Cu_x$ films occurs by the flacking mechanism. In this case, an in-crease in the thickness of the amorphous $Zr_{1-x}Cu_x$ layer and Cu content x lead to an increase in the critical fluence from 5 × 10_{17} cm_{-2} to 8 × 10^{17} cm_{-2}.

Declaration of competing interest

The authors declare that they have no known competing financial interests or personal relationships that could have appeared to influence the work reported in this paper.

Acknowledgments

This work was supported by the French government program “Investissements d'Avenir” (EUR INTREE, reference ANR-18-EURE-0010). The SRIM calculations are carried out at Tomsk Polytechnic University within the framework of Tomsk Polytechnic University Competitive-ness Enhancement Program grant. The authors also acknowledge the fi-nancial support from the Education Ministry of Republic of Belarus (2022) .

Appendix A. Supplementary data

Supplementary data to this article can be found online at https://doi.org/10.1016/j.surfcoat.2022.128547.

References

[1] M.J. Demkowicz, D. Bhattacharyya, I. Usov, et al., The effect of excess atomic volume on he bubble formation at fcc–bcc interfaces, Appl. Phys. Lett. 97 (2010) 161903, https://doi.org/10.1063/1.3502594.
[2] M.J. Demkowicz, A. Misra, A. Caro, The role of interface structure in controlling high helium concentrations, Curr. Opin. Solid State Mater. Sci. 16 (2012) 101–108, https://doi.org/10.1016/j.cossms.2011.10.003.
[3] Z. Jiao, G.S. Was, The role of irradiated microstructure in the localized deformation of austenitic stainless steels, J. Nucl. Mater. 407 (2010) 34–43, https://doi.org/10.1016/j.jnucmat.2010.07.006.
[4] R.E. Baumer, M.J. Demkowicz, Radiation response of amorphous metal alloys: subcascades, thermal spikes and super-quenched zones, Acta Mater. 83 (2015) 419–430, https://doi.org/10.1016/j.actamat.2014.10.020.
[5] R.W. Grimes, R.J.M. Konings, L. Edwards, Greater tolerance for nuclear materials, Nat. Mater. 7 (9) (2008) 285–683, https://doi.org/10.1038/nmat2266.
[6] Xinghang Zhang, Khalid Hattar, Youxing Chen, et al., Radiation damage in nanostructured materials, Prog.Mat. Sc. 96 (2018) 217–321, https://doi.org/10.1016/j.pmatsci.2018.03.002.
[7] O. El-Atwani, K. Hattar, J. Hinks, et al., Helium bubble formation in ultrafine and nanocrystalline tungsten under different extreme conditions, J. Nucl. Mater. 458 (2015) 216–223, https://doi.org/10.1016/j.jnucmat.2014.12.095.
[8] K. Yu, Y. Liu, C. Sun, et al., Radiation damage in helium ion irradiated nanocrystalline Fe, J. Nucl. Mater. 425 (2012) 140–146, https://doi.org/10.1016/j.jnucmat.2011.10.052.
[9] I. Kim, L. Jiao, F. Khatkhatay, et al., Size-dependent radiation tolerance in ion irradiated TiN/AlN nanolayer films, J. Nucl. Mater. 441 (2013) 47–53, https://doi.org/10.1016/j.jnucmat.2013.05.035.
[10] D. Chen, N. Li, D. Yuryev, et al., Self-organization of helium precipitates into elongated channels within metal nanolayers, Sci. Adv. 3 (11) (2017) eaao2710, https://doi.org/10.1126/sciadv.aao2710.
[11] X. Zhang, K. Hattar, Y. Chen, et al., Radiation damage in nanostructured materials, Prog. Mater. Sci. 96 (2018) 217–321, https://doi.org/10.1016/ j.pmatsci.2018.03.002.
[12] A. Misra, M. Demkowicz, X. Zhang, et al., The radiation damage tolerance of ultra-high strength nanolayered composites, JOM 59 (2007) 62–65, https:// doi.org/10.1007/s11837-007-0120-6.
[13] E.G. Fu, A. Misra, H. Wang, et al., Interface enabled defects reduction in helium ion irradiated Cu/V nanolayers, J. Nucl. Mater. 407 (2010) 178–188, https:// doi.org/10.1016/j.jnucmat.2010.10.011.
[14] N. Li, M.S. Martin, O. Anderoglu, et al., He ion irradiation damage in Al/Nb multilayers, J. Appl. Phys. 105 (2009) 123522, https://doi.org/10.1063/1.3138804.
[15] N. Li, J.J. Carter, A. Misra, et al., The influence of interfaces on the formation of bubbles in He-ion-irradiated Cu/Mo nanolayers, Philos. Mag. Lett. 91 (2011) 18–28, https://doi.org/10.1080/09500839.2010.522210.
[16] N. Li, E.G. Fu, H. Wang, et al., He ion irradiation damage in Fe/W nanolayer

films, J. Nucl. Mater. 389 (2009) 233–238, https://doi.org/10.1016/j.jnucmat.2009.02.007.
[17] A.J. Van Vuuren, A. Sohatsky, V.V. Uglov, et al., The effect of helium irradiation on the thermal evolution of the microstructure of nc-ZrN, Phys. Status Solidi C 13 (2016) 886–889, https://doi.org/10.1002/pssc.201600027.
[18] V.V. Uglov, G. Abadias, S.V. Zlotski, et al., Surface blistering in ZrSiN nanocomposite films irradiated with He ions, Surf. Coat. Technol. 394 (2020) 125654, https://doi.org/10.1016/j.surfcoat.2020.125654.
[19] V.V. Uglov, G. Abadias, S.V. Zlotski, et al., Blister formation in ZrN/SiN multilayers after He irradiation, Surf. Coat. Technol. 344 (2018) 170–176, https://doi.org/10.1016/j.surfcoat.2018.02.095.
[20] V.V. Uglov, N.T. Kvasov, G.E. Remnev, et al., Size effect in AlN/SiN multilayered films irradiated with helium and argon ions, Nucl. Instr. Meth. Phys. Res. 435 (2018) 228–235, https://doi.org/10.1016/j.nimb.2018.01.012.
[21] V.V. Uglov, G. Abadias, S.V. Zlotski, et al., Tolerance of MeN/Si_3N_4 (Me=Zr, Al, Cr) multilayered systems to radiation erosion, Surf. Coat. Technol. 399 (2020) 126146, https://doi.org/10.1016/j.surfcoat.2020.126146.
[22] J. Zhang, Y. Wang, X. Liang, et al., Size-dependent He-irradiated tolerance and plastic deformation of crystalline/amorphous Cu/Cu–Zr nanolaminates, Acta Mater. 92 (2015) 140–151, https://doi.org/10.1016/j.actamat.2015.03.055.
[23] K.Y. Yu, Z. Fan, Y. Chen, et al., In situ observation of defect annihilation in Kr ion-irradiated bulk Fe/amorphous-Fe_2Zr nanocomposite alloy, Mater. Res. Lett. 3 (2014) 35–42, https://doi.org/10.1080/21663831.2014.951494.
[24] G. Abadias, V.V. Uglov, I.A. Saladukhin, et al., Growth, structural and mechanical properties of magnetronsputtered ZrN/SiN_x nanolaminated coatings, Surf. Coat. Technol. 308 (2016) 158–167, https://doi.org/10.1016/j.surfcoat.2016.06.099.
[25] http://www.srim.org.
[26] M. Apreutesei, P. Djemia, L. Belliard, et al., Structural-elastic relationships of Zr-TL (TL Cu, Co, Ni) thin films metallic glasses, J. Alloys Compd. 707 (2017) 126–131, https://doi.org/10.1016/j.jallcom.2016.12.208.
[27] M. Ghidelli, A. Orekhov, A. Li Bassi, et al., Novel class of nanostructured metallic glass films with superior and tunable mechanical properties, Acta Mater. 213 (2021) 116955, https://doi.org/10.1016/j.actamat.2021.116955.
[28] B.R. Braeckman, D. Depla, On the amorphous nature of sputtered thin film alloys, Acta Mater. 109 (2016) 323–329, https://doi.org/10.1016/j.actamat.2016.02.035.
[29] D. Ma, A. D. Stoica and X.-L. Wang, Power-law scaling and fractal nature of medium-range order in metallic glasses, Nat. Mater. 8 30–34. doi: https://doi.org/10.1038/NMAT2340.
[30] K. Saksl, H. Franz, P. Jóvári, et al., Evidence of icosahedral short-range order in $Zr_{70}Cu_{30}$ and $Zr_{70}Cu_{29}Pd_1$ metallic glasses, Appl. Phys. Lett. 83 (2003) 3924–3926, https://doi.org/10.1063/1.1626266.
[31] V.V. Uglov, G. Abadias, S.V. Zlotski, et al., Blistering in helium-ion-irradiated zirconium, aluminum, and chromium nitride films, journal of surface investigation: X-ray, synchrotron and neutron, Techniques 14 (2020) 359–365, https://doi.org/ 10.1134/S1027451020020524.
[32] Q. Su, S. Inoue, M. Ishimaru, et al., Helium irradiation and implantation effects on the structure of amorphous silicon oxycarbide, Sci. Rep. 7 (2017) 3900(1–8), https://doi.org/10.1038/s41598-017-04247-x.
[33] P. Coddet, F. Sanchette, J.C. Rousset, et al., On the elastic modulus and hardness of co-sputtered Zr–Cu–(N) thin metal glass films, Surf. Coat. Technol. 206 (2012) 3567–3571, https://doi.org/10.1016/j.surfcoat.2012.02.036.